Energy Science & Engineering

ORIGINAL ARTICLE OPEN ACCESS

Numerical and Experimental Investigation of Gas Turbine Rotor for Early Fault Detection

Muhammad Akhtar[1] | Waqar Muhammad Ashraf[2] | Nasir Hayat[1] | Ghulam Moeen Uddin[1] | Fahid Riaz[3]

[1]Department of Mechanical Engineering, University of Engineering and Technology, Lahore, Punjab, Pakistan | [2]The Sargent Centre for Process Systems Engineering, Department of Chemical Engineering, University College London, London, UK | [3]College of Engineering, Abu Dhabi University, Abu Dhabi, UAE

Correspondence: Muhammad Akhtar (makhtar2389@gmail.com) | Fahid Riaz (fahid.riaz@u.nus.edu)

Received: 13 August 2024 | **Revised:** 20 February 2025 | **Accepted:** 24 February 2025

Keywords: fault detection | gas turbine | harmonic analysis | modal analysis | vibration analysis

ABSTRACT

Rotodynamic analysis is a key analysis for turbomachinery for investigating the health and integrity of equipment. Most of the analyses are performed at the design stage, while the actual machine behavior is different due to imperfections like unbalance, misalignment, cracks, and so forth. In this paper, a representative CAD model of a gas turbine rotor is developed to get the actual rotodynamic response of a rotor. Vibration data of the rotor is compared with that of the developed numerical model. The reference model representation of the actual machine in terms of critical speed and vibration value is found to be 99.7% and 99.1%, respectively. Rotodynamic analyses of numerical models are performed for early identification of faults under various scenarios of unbalance, crack, and crack with unbalance. For these scenarios, modal analysis and harmonic analysis are performed. Natural frequencies and vibration behavior are utilized to capture the variation that indicates the presence of a fault. This way, early identification of faults is made to save the machine from damage. Within the unbalance range of 1.0×10^{-9} to 0.5 kg, a direct relation between change in unbalance mass and vibration amplitude is observed in the case of unbalance and unbalance with crack. Similarly, for cracks (of 1–3 mm thickness and depth up to 372 mm), a shift in maximum vibration amplitude frequency to first critical speed from second critical speed is noted. Hilbert transform is utilized to track the nonlinearity especially up to an operating speed of 3000 rpm (50 Hz). These key outcomes can be used to reduce rotary machine downtime by not only highlighting the problem at a very early stage but also swiftly identifying its root cause for the smooth working of rotary equipment in the industry.

1 | Introduction

Early fault finding is a major challenge in turbomachinery, especially once these are installed at their locations and are in operation. The deviations of design and actual operating conditions include a certain degree of unbalance in the real machine since its first start, cracks development due to harsh environment, and other issues in the machines [1]. Development of a representative model incorporating these deviations into account and subsequent model-validation is a quite tricky, difficult and time taking task [2]. A procedure for machine-specific model development, validation, and harmonic analysis is carried out for feature extraction that can be used for early fault detection in the rotary equipment. However, the failure of dynamic behavior prediction in the industrial environment may cause damage to the health and integrity of the rotary equipment leading to commercial loss and shutdown of industrial operation [3]. Therefore, industrial and research community

Abbreviations: 1S1B, first stage first blade; 1S2B, first stage second blade; 1S3B, first stage third blade; 2S1B, second stage first 1blade; 2S2B, second stage second blade; B, blade; Comp., compressor; FEA, finite element analysis; FEM, finite element method; FIV, flow induced vibration; GT, gas turbine; m/s, meter per second; S, stage.

develop different predictive models capturing the dynamic operating characteristics of rotary equipment to predict the crack initiation and propagation, and health of the equipment is monitored in real-time to ensure the smooth performance of rotary equipment.

The health and equipment integrity are critical to ensure the smooth operation of industrial complexes in the dynamic mode of operation. An extensive literature review was conducted to identify the latest techniques being developed and deployed for health monitoring and assessing equipment integrity. Rotor modeling and analysis of industrial rotors is performed to find mode shapes and natural frequencies. Comparison of rotodynamic properties of new rotor and rotor having wear is made to identify the impact of wear on critical speed and vibration amplitude. It was found that natural frequency decreases while vibration amplitude increases in case of wear [4]. Comparison of rotodynamic properties of straight and curved blades of a gas turbine is also made. It was observed that the natural frequency of a straight blade increased with twisting, and an increase in natural frequency was observed with an increase in rotational speed [5].

Vibration diagnosis method detectability for gas turbine blade cracks was improved by utilizing the feature of structural element having crack and change in damping characteristics [6]. The factors like mode shapes, natural frequencies, and unbalances response have also been meticulously considered in the machine's design [7]. Model validation is a key requirement before any kind of analysis and analysis-based results [8]. Compressor dynamic model is developed for the identification of surge [9], and review of turbomachinery vibration causes, and their identification is discussed in [10].

Experimental validation of unbalance response of rotor was studied by using the Kalman filter as an input. The devised method can be used for online identification of unbalance in rotating shaft assuming its speed is not varied [11]. Causes of vibrations in combined cycle power plants, detection techniques and the tools used for vibration analysis are reviewed in [12]. Symplectic superposition method was applied for free vibration analysis of cracked plate and the same can be applied to rotor blades. Results obtained from such analyses and finite element method (FEM) were in good agreement. It was also shown that crack length has definite impact on natural frequencies and mode shapes [13–15]. Vibration analysis was performed for the detection of unbalanced forces in rotors that can cause cracks to form and grow over time [16]. The numerical results were found to match closely with those obtained through analytical methods, with a maximum deviation of 7.31% for the critical speed.

Operational modal analysis of power industry rotating machines with support was performed to get an idea of unbalance, mode shapes and natural frequency [17]. Many studies have been done to avoid the damage done to the rotor while passing through critical speed zones, especially when operating speed is beyond first and second critical speed zones [18]. Calculative and experimental analysis of natural and critical frequencies and mode shapes of high-speed rotor for micro gasturbine plant was performed [19]. Modal analysis is used for identifying shapes of the modes of different models and natural frequencies [20]. Common models include Coulomb friction and damping, softening and hardening cubic stiffness, saturation, bilinear stiffness, and clearance [21].

It was observed that as the crack depth increases, the orbit size and response increase while the critical speed decreases [22]. FEM was used for vibration analysis of cracked beam. Elements of beam were modeled as springs of varying stiffness as per crack depth. Results indicated that natural frequency was decreased because of loss in beam flexibility due to crack [23]. Prediction of cracks in the gas turbine by using image processing and deep learning methodologies was made with 96% accuracy [24]. One of the abnormalities in the turbine rotors is initiation and propagation of blade cracks. Finite integral transform (FIT) method was proposed as an alternative to find free vibration of crack section [25]. Extended FEM was implied for the frequency response analysis to identify crack [26]. Modular kit was employed for experimentation, and the outcome confirmed the existence of different motion patterns like synchronous, sub-synchronous and whirling [27]. Feature extraction from subcritical zone in the transient state was done to identify the crack and misalignment. It was found that using the sub-critical startup response can effectively identify faults in a cracked rotor [28].

The frequency patterns were examined for fault analysis using the Hilbert transform method [29]. The results of the study indicated that the various compositions of the modulation frequency can be employed to identify local faults such as rub, crack and rub-crack in coupled rotor systems [30]. Dynamic behavior of gas turbine with increase in speed was studied and it was found that at lower speed system behaves like a single cycle motion, while at higher speed, it performs like two cycle motion [31]. This bifurcation of motion provides useful information for reliable design of rotary equipment.

A comprehensive literature review conducted on a range of fault detection, prediction and mitigation techniques reveals that as the actual operating conditions for the working of the machine change over time, the dynamic rotodynamic profiles of the machine change significantly, leading to instability and unsafe mode of operation of the equipment. There is a need to develop a model that depicts the machine's actual behavior in real-time to make early fault prevention schemes and strategies to ensure the smooth operation of equipment. This research paper addresses the potential research gap on making an adaptive and response model representing the working of the equipment in real-time conditions. The comparison of the developed model is made with the actual model installed in industry to quantify the accuracy of the developed model. Later, performance assessment analyses are performed while simulating different anomalies in the developed model to predict the response of model in case of anomaly that can provide early warnings to take mitigation steps for fault removal and maintain the smooth operation of equipment. The representative model development of the gas turbine rotor and the performance comparison with the actual gas turbine rotor can help the industrial practitioner to make early maintenance schemes and operate the equipment safely for the smooth operation of industrial complexes.

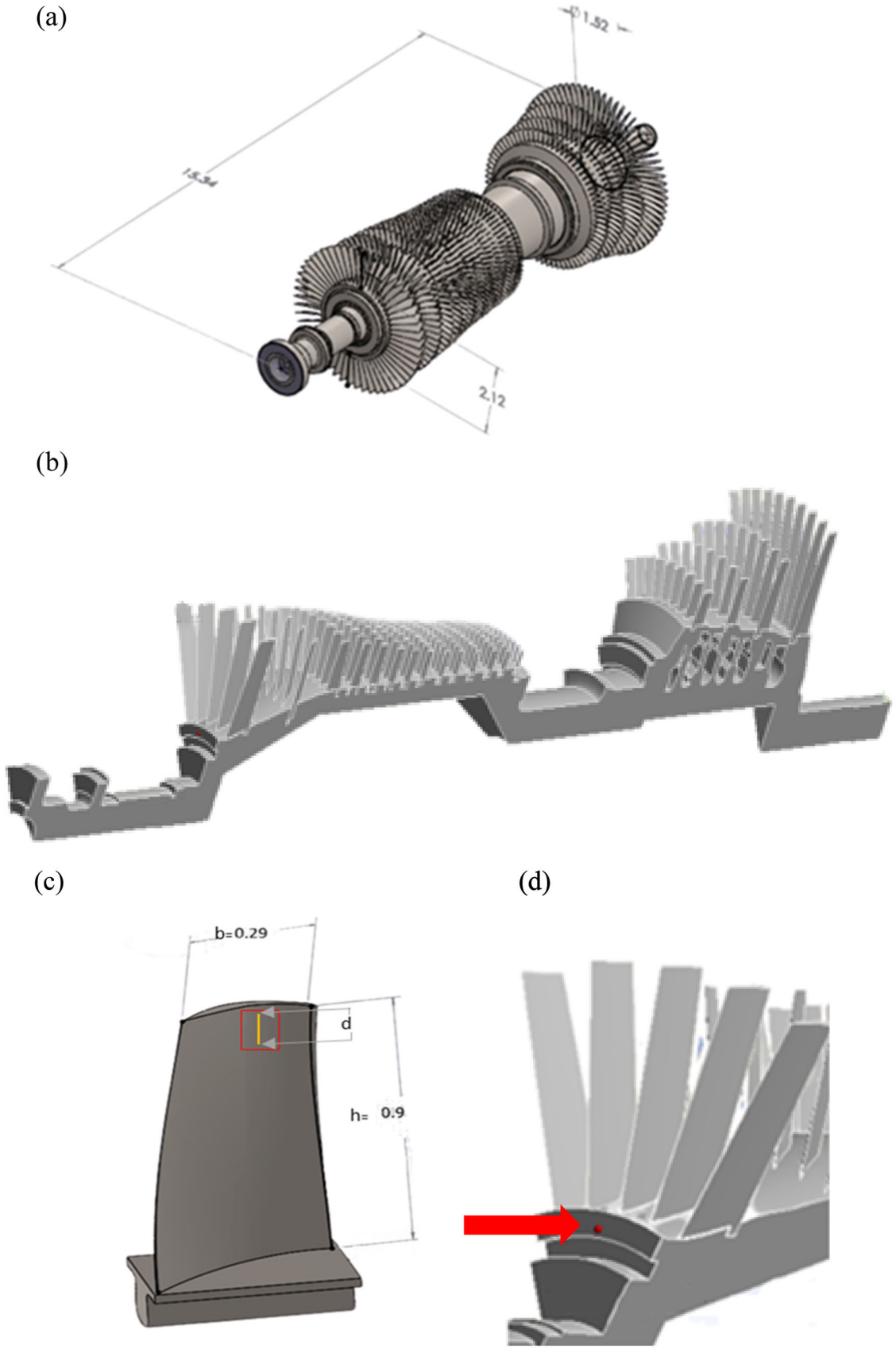

FIGURE 1 | The developed gas turbine model: (a) complete rotor model with dimensions; (b) 1/8th section of rotor model; (c) blade and crack dimensions; (d) closeup view of model with unbalance mass location (shown as red dot).

2 | Methodology

Gas turbine model developed in SOLIDWORKS is shown in Figure 1a, while the dimensional details of the equipment mentioned in Table 1 were used for the current analysis. Each component, that is, blades, and rotor were developed and assembled before import into ANSYS workbench for further analyses after fine meshing. 1/8th of this rotor model (see Figure 1b)was analyzed by taking advantage of the model symmetry to speed up the computational analyses. Dimensional details of the sample blade are shown in Figure 1c. After import of model into ANSYS, Modal Analysis of rotor was performed at different speed levels (1000, 1500 and 3000 rpm) while selecting the first 30 modes of each speed level to get the critical speed ranges for comparison with the critical speed range of the actual machine. The actual machine is an operational 400 MW gas turbine (GT) having vibration monitoring system installed on it for monitoring and protection.

Actual machine vibration amplitude was checked at various (1X, 2X and 3X) modes by taking data from vibration monitoring system. Similarly, vibration amplitude and critical speed ranges were analyzed from start-up pattern of the actual machine. Unbalance-mass addition was done to the 1/8 rotor model to get closer values of critical speed ranges and vibration amplitudes (in the form of velocity) as of the actual machine. After a lot of iterations, the finalized value of unbalance mass and its location was obtained as shown in Figure 1d. This model with inherent unbalance mass was considered as reference model. Campbell diagram of the reference model was obtained from Modal analysis.

Hairline crack was simulated in distinct locations (different blades on same stages, same stage but different blade and different blade and different stage) of reference model to get the behavior of model with crack and model having crackwith unbalance mass. Different sizes (different crack thickness and depth), orientations (horizontal, vertical) and locations (top, middle and bottom) of cracks were selected for analysis but ultimately the top side vertical hairline crack having 1 mm thickness and 93 mm depth was selected for further analyses due its better response to abnormalities/abnormal conditions.

Modal and Harmonic analyses were performed on the reference model to obtain mode shapes, natural frequencies, and vibration patterns. Mode shapes of the reference model were analyzed, and the modes with the maximum difference in frequency and total deformation at various speed levels were identified. Investigation regarding mode creation, dwindling and shifting for different cases, as mentioned in Table 2 was carried out. Modal and Harmonic analyses were performed on the models with different simulated abnormalities. Only maximum vibration graphs were compared to get fruitful results. Summary of analyses performed is given below in Table 2.

TABLE 1 | Numerical model characteristics.

Material	Structural steel
Length $X \times Y \times Z$	1.52 m × 2.12 m × 15.34 m
Density	7850 kg/m^3
Number of nodes	88,589
Elements	43,951
Compressive/tensile yield strength	2.5×10^2 MPa
Young's modulus	210,000 MPa
Poison's ratio	0.3

Each harmonic response case was analyzed for vibration amplitude, vibration amplitude frequency, and change in vibration amplitude frequency from reference model. Harmonic response of models with cracks of various thickness (1, 2, and 3 mm) and crack depths(minimum 31 mm, maximum 403 mm, increment 31 mm) at various locations (top, middle and bottom) were analyzed.

Nonlinearity analysis was done by using Hilbert Transform. Uncertainty analysis was also done by changing the material properties to see the impact on natural frequency.

3 | Results and Discussion

The purpose of this phase of work was to perform the rotor dynamic analyses of a gas turbine representative ANSYS model and its prospective behavior in case of anomalies like unbalance and crack. The results demonstrated a positive correlation between unbalance mass and vibration amplitude. The analyses further identified dominance of crack behavior over unbalance behavior. The results support the theories and previous work of vibration analysis. One of the findings that contradicts the previous work was shifting of the maximum vibration amplitude frequency from second critical speed range to first critical speed range in the cases of crack and crack with unbalance while overall vibration pattern remained the same.

3.1 | Convergence of ANSYS Model

Convergence of natural frequency results with number of elements is shown in Figure 2. Reason behind the selection of tetrahedron element type and fine meshing was to get better convergence and to get the best results for the work. If coarse meshing is selected, the results may differ and may not represent the actual behavior. Further reduction of element size resulted in a drastic increase in calculation time, but the results were the same, indicating that the current selection is optimum in terms of analysis time and results quality.

As per the above results, convergence in output of analysis is well converged if about 43,000 elements of model are selected, and number of modes are 18. Convergence of results is necessary. In ANSYS modeling and analysis, if the number of elements is increased, computation time is much increased. Similarly, if the number of elements is reduced, this reduces the computation, but at a certain level, if the number of elements is further reduced, it impacts the results. From the above graph, it is evident that if the number of elements is 43,000, the results would be accurate. Lesser than this number, accuracy would be

TABLE 2 | List of cases for analyses.

Description	Cases
Models with unbalance mass (From 1.0×10^{-9} to 0.05 kg)	i. Models with unbalance mass
Models with crack and without unbalance mass (stages, $i = 1,2$/Blades, $j = 1,2$)	ii. Models with crack as per specified range
Model with unbalance and crack (stages, $i = 1,2,3$/blades $j = 1,2,3$/Unbalance mass (From 1.0×10^{-9} to 0.05 kg)	iii. Models with unbalance and crack as per stated range

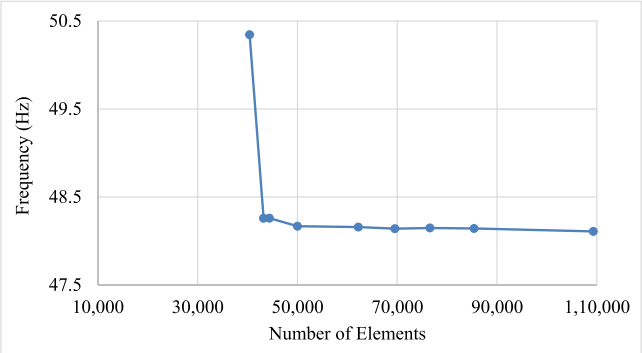

FIGURE 2 | Convergence of results obtained frequency versus number of elements in the model.

impacted and at more than this number of elements, computation time would be increased with not many improvements in the results. That is, in the current work, the elements selected for analysis were more than 43,000 and the number of modes selected was 30. This was done to ensure accuracy, although computation time was increased.

3.2 | Comparison of Numerical Model With Actual Machine

The vibration pattern of the actual machine at various operating modes is shown in Figure 3. Vibration amplitude is maximum at 1×, that is, first mode. So, it can be said that the machine is already in unbalance condition. Results of actual machine and reference model parameters are tabulated below in Table 3. As parameters (critical speeds and vibration amplitude) of actual machine and numerical model are corresponding with each other so, the reference model represents the behavior of actual machine.

Modal validation of developed ANSYS model with actual machine was also performed in [19]. It was found that the deviation of critical speed of model from actual machine was 2.1% while in the current work, maximum deviation in critical speed was 0.3%, demonstrating the accuracy of the developed model to represent the true operating behavior of equipment in the real-time operating conditions. The reason for better accuracy is 30 modes were selected for modal analysis in the current work; while in [19], 16 modes were selected for modal analysis. Similarly, minimum error between solid works model and beam model was 2.13 [32]. In [22], critical speed deviation of analytical and numerical models was 7.31% [15]. So, it can be said that deviation of current work is lesser than already accepted and published work. Hence, the developed model is validated and its

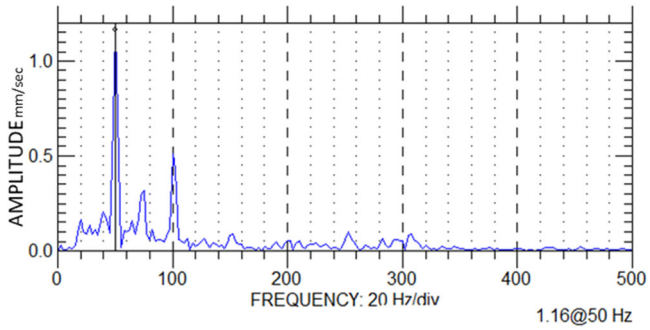

FIGURE 3 | Actual machine vibration pattern at various modes.

response to any simulated anomaly would be considered as actual machine response to that anomaly. This type of work can be considered as a non-destructive testing technique. Model true representation of the actual machine is particularly important as simulation models are approximate imitations of real-world systems, and they will not provide good results if not accurate.

3.3 | Reference Model Critical Speed Analysis

Campbell diagram results of gas turbine rotor model at various speed levels (1000, 1500 and 3000 rpm) are shown in Table 4. It is evident from the results that the first critical speed range of model is from 1740 to 1944 rpm while the second critical speed range is from 2561 to 2895 rpm. Further, it was noted that critical speed in case of forward whirl is increased with increase in operating speed while it is decreased for backward whirl.

The same method of finding critical speed was used for critical speed analysis of sealing machine [7]. Modal analysis of sealing machine rotor was carried out for calculation of modal parameters and identification of critical speed [7]. The same method was followed for critical speed identification in the current work.

The critical speeds were observed far from the operating speed which is sign of good machine design. The identification of critical speed is important for proper design and operation of equipment. If operating range is near to critical speed, higher vibration amplitude would be observed. That's why critical speed ranges of machines are kept much different than operating speed. Appearance of 1X component as high amplitude points to unbalance while 2X points to crack [30]. 2X component is feature of crack in high vibration analysis.

Further analysis revealed that in case of forward whirl, the critical speed (natural frequency) was directly related to

TABLE 3 | Comparison of actual machine parameters with numerical model parameters.

Parameter	Actual machine result	ANSYS model result	% deviation
First critical speed range	1810 to 1950 rpm	1740 to 1944 rpm	0.3
Second critical speed range	2575 to 2900 rpm	2561 to 2895 rpm	0.1
Vibration amplitude (mm/s)	10.8	10.9	0.9

TABLE 4 | Campbell diagram values of reference model.

		Reference model			
Mode	Whirl direction	Critical speed (RPM)	1000 rpm (Hz)	1500 rpm (Hz)	3000 rpm (Hz)
6.	BW	1740.8	29.172	29.082	28.66
7.	FW	1895.2	31.578	31.584	31.597
8.	BW	1899.1	31.653	31.653	31.652
9.	BW	1906	31.768	31.768	31.765
10.	FW	1912.5	31.842	31.859	31.915
11.	FW	1932.5	32.195	32.203	32.222
12.	FW	1944.4	32.347	32.367	32.499
13.	FW	2561.8	42.699	42.699	42.699
14.	BW	2586.7	43.118	43.117	43.109
15.	BW	2600.9	43.355	43.354	43.346
16.	BW	2620.9	43.698	43.696	43.677
17.	BW	2633.4	43.914	43.91	43.882
18.	BW	2653.3	44.303	44.289	44.201
19.	BW	2761.7	47.111	46.83	45.878
20.	BW	2870.5	47.848	47.845	47.842
21.	FW	2895.0	48.247	48.248	48.25

operating speed, that is, increases with increase in operating speed. Similar results of forward and backward whirl with increase in speed was observed in [32]. This was due to gyroscopic effect. Rotordynamic experimentation was done for whirl analysis [27]. For example, as mode 7 natural frequency was forward whirl, natural frequency at 3000 rpm was more than natural frequency of the same mode at 1000 rpm. This was because of same direction of whirl and rotor rotation as these two directions complemented each other. Similarly, for a backward whirl, the inverse relation between two parameters was observed. This was due to opposite directions of whirling motion and rotor rotation. For example, as mode 6 natural frequency was backword whirl, natural frequency at 3000 rpm was 28.66 Hz and lesser than natural frequency of the same mode at 1000 rpm which was 29.172 Hz. This was because of opposite direction of whirl and rotor rotation as these two directions oppose each other.

3.4 | Comparative Analysis of Total Deformation for Different Models

Total deformation and frequency results of different models against each mode are presented in Table 5. Sample screenshots of mode shapes, frequency and deformation value are shown in Figure 4. In reference model, most of the frequency and deformation values of each mode at different rotational velocity are matching. Natural frequency is increased as number of modes are increased. Within operating speed (up to 50 Hz), maximum change in frequency with respect to rotational velocity was observed at mode#19. Decrease in natural frequency with increase in rotational velocity was observed at mode#19. Further to this, increase in natural frequency with increase in rotational velocity was observed at mode#24 and 25. Similarly, increase in deformation with increase in rotational velocity was noted at mode#10 while opposite behavior was observed at mode#12, 19 and 23. Decrease in deformation was observed with increase in natural frequency at mode# 18, 19, 20 and 23, 24, 25.

Newmodes generation was observed due to crack in different models of crack. These new modes have different mode shape and natural frequencies but in continuation of existing natural frequencies. Some modes diminished also due to generation of these new modes. Sixnew modes were generated for first stage crack model while seven new modes were generated for the second and third stage crack models. Similarly, shifting of modes was also observed due to crack. Reference model mode shapes of mode#6, 8, 17, 19 and 23 were shifted to mode#7, 10, 16, 18 and 22 of first stage crackmodel. Furthermore, reference model mode shapes of mode#17, 19, 20, 23 and 27 were shifted to mode#16, 18, 19, 20 and 30 of second stage crack model.

TABLE 5 | Frequency and deformation against each mode for different cases.

Reference model values				Comp. stage 1 crack		Comp. stage 2 crack		Comp stage 3 crack	
Rot. Vel.	**Mode #**	**Freq (Hz)**	**Deformation (m)**	**Freq (Hz)**	**Deformation (m)**	**Freq (Hz)**	**Deformation (m)**	**Freq (Hz)**	**Deformation (m)**
1000 rpm	1	4.2421	0.01052	4.2692	0.01049	4.2692	0.01049	4.2693	0.01049
	2	6.3971	0.00897	7.0687	0.00949	7.0709	0.00950	7.0711	0.00949
	3	12.26	0.01859	12.395	0.01866	12.395	0.01868	12.398	0.01868
	4	13.622	0.01246	14.655	0.01394	14.663	0.01324	14.663	0.01328
	5	16.521	0.02995	16.561	0.03599	16.566	0.02965	16.566	0.02987
	6	29.172	0.03782	27.037	0.39168	29.325	0.03925	29.327	0.04145
	7	31.578	0.28968	29.393	0.03664	31.545	0.35010	31.556	0.30640
	8	31.653	0.26176	31.553	0.27487	31.688	0.31258	31.6	0.31854
	9	31.768	0.26892	31.594	0.31166	31.813	*0.28506*	31.705	0.20585
	10	31.842	0.20845	31.773	0.23855	31.825	0.19036	31.765	0.25065
	11	32.195	0.27334	32.09	0.06445	32.188	0.25690	32.087	0.25512
	12	32.347	0.31430	34.835	0.39534	32.312	0.25850	32.253	0.16841
	13	42.699	0.46837	42.636	0.47212	42.617	0.47251	42.599	0.47121
	14	43.118	0.43285	43.071	0.44301	43.068	0.43606	43.008	0.44522
	15	43.355	0.42785	43.415	0.44571	43.378	0.43829	43.378	0.45120
	16	43.698	0.41995	44.058	0.34178	44.157	0.38387	44.055	0.37668
	17	43.914	0.36387	44.328	0.32545	44.427	0.36990	44.256	0.33679
	18	44.303	0.36127	47.114	0.25660	47.119	0.23927	44.7	0.42849
	19	47.111	0.14093	47.54	0.37019	47.553	0.37855	47.199	0.24280
	20	47.848	0.43291	47.808	0.33692	47.752	0.38147	47.642	0.37286
	21	48.247	0.39362	47.917	0.25291	47.898	0.27287	47.96	0.38726
	22	48.419	0.32618	48.101	0.27517	48.102	0.28442	48.221	0.35600
	23	48.736	0.34871	48.531	0.34445	48.543	0.36591	48.592	0.33831
	24	56.095	0.05604	56.243	0.05755	56.237	0.05738	56.19	0.05435
	25	61.381	0.01580	63.073	0.01757	63.076	0.01926	63.075	0.01768
	26	68.452	0.62678	69.993	0.61432	69.947	0.61295	69.889	0.61417
	27	70.744	0.59211	70.864	0.49060	70.754	0.49535	70.81	0.45618
	28	70.915	0.45883	71.083	0.45673	70.988	0.46603	71.023	0.41986
	29	71.029	0.42879	71.712	0.45611	71.645	0.49089	71.624	0.47797

(Continues)

TABLE 5 | (Continued)

	Reference model values			Comp. stage 1 crack		Comp. stage 2 crack		Comp stage 3 crack	
Rot. Vel.	**Mode #**	**Freq (Hz)**	**Deformation (m)**	**Freq (Hz)**	**Deformation (m)**	**Freq (Hz)**	**Deformation (m)**	**Freq (Hz)**	**Deformation (m)**
	30	71.256	0.43260	71.94	0.37953	71.882	0.42328	71.863	0.41364
1500 rpm	1	4.2369	0.01051	4.2647	0.01048	4.2647	0.01048	4.2648	0.01048
	2	6.3948	0.00895	7.0629	0.00948	7.065	0.00948	7.0652	0.00948
	3	12.225	0.01834	12.364	0.01855	12.364	0.01858	12.367	0.01858
	4	13.551	0.01235	14.566	0.01377	14.574	0.01306	14.574	0.01310
	5	16.578	0.02959	16.634	0.03534	16.64	0.02907	16.64	0.02928
	6	29.082	0.03708	27.036	0.39153	29.23	0.03847	29.232	0.04050
	7	31.584	0.29564	29.299	0.03693	31.549	0.35553	31.561	0.31576
	8	31.653	0.26075	31.556	0.27656	31.69	0.32079	31.601	0.31557
	9	31.768	0.27371	31.594	0.31124	31.814	0.31889	31.706	0.20177
	10	31.859	0.23196	31.77	0.23899	31.843	0.23615	31.778	0.25497
	11	32.203	0.25507	32.145	0.05761	32.187	0.24043	32.083	0.25159
	12	32.367	0.28884	34.835	0.39531	32.342	0.22878	32.292	0.15204
	13	42.699	0.46852	42.636	0.47226	42.617	0.47265	42.599	0.47136
	14	43.117	0.43304	43.07	0.44330	43.067	0.43641	43.007	0.44548
	15	43.354	0.42863	43.413	0.44622	43.376	0.43885	43.377	0.45167
	16	43.696	0.41986	44.055	0.34350	44.155	0.38212	44.054	0.37392
	17	43.91	0.36514	44.318	0.32797	44.416	0.36737	44.25	0.33422
	18	44.289	0.36550	46.849	0.16879	46.848	0.15773	44.687	0.43042
	19	46.83	0.10625	47.503	0.41639	47.522	0.41811	46.93	0.16408
	20	47.845	0.43934	47.805	0.35576	47.752	0.37587	47.614	0.41189
	21	48.248	0.38765	47.904	0.30858	47.883	0.34971	47.957	0.39484
	22	48.422	0.31847	48.108	0.29216	48.112	0.30968	48.224	0.34346
	23	48.789	0.33244	48.605	0.32185	48.612	0.34301	48.654	0.32243
	24	56.61	0.05726	56.78	0.05386	56.775	0.05377	56.731	0.05324
	25	61.616	0.01557	63.286	0.01741	63.289	0.01909	63.289	0.01752
	26	68.457	0.62651	69.996	0.61375	69.949	0.61232	69.892	0.61363
	27	70.745	0.59153	70.864	0.49003	70.754	0.49314	70.81	0.45690
	28	70.915	0.45861	71.089	0.45505	70.995	0.46263	71.029	0.41941

(Continues)

TABLE 5 | (Continued)

Reference model values				Comp. stage 1 crack		Comp. stage 2 crack		Comp stage 3 crack	
Rot. Vel.	**Mode #**	**Freq (Hz)**	**Deformation (m)**	**Freq (Hz)**	**Deformation (m)**	**Freq (Hz)**	**Deformation (m)**	**Freq (Hz)**	**Deformation (m)**
	29	71.029	0.43098	71.712	0.45604	71.645	0.48952	71.624	0.47698
	30	71.259	0.43323	71.947	0.37814	71.888	0.42053	71.87	0.41124
3000 rpm	1	4.2091	0.01044	4.2404	0.01043	4.2405	0.01042	4.2405	0.01043
	2	6.3825	0.00887	7.0319	0.00942	7.0338	0.00943	7.034	0.00943
	3	12.037	0.01690	12.2	0.01799	12.2	0.01802	12.203	0.01802
	4	13.227	0.01189	14.18	0.01327	14.187	0.01254	14.187	0.01259
	5	16.838	0.02826	16.944	0.03349	16.949	0.02732	16.949	0.02751
	6	28.66	0.03460	27.026	0.39040	28.793	0.03573	28.795	0.03720
	7	31.597	0.31129	28.868	0.04766	31.558	0.36784	31.573	0.33396
	8	31.652	0.25625	31.566	0.28135	31.694	0.33761	31.604	0.29959
	9	31.765	0.28354	31.594	0.30950	31.811	0.33252	31.705	0.22997
	10	31.915	0.29583	31.758	0.24135	31.9	0.28954	31.822	0.26825
	11	32.222	0.27723	32.378	0.03912	32.183	0.27922	32.067	0.24799
	12	32.499	0.18288	34.833	0.39517	32.502	0.14541	32.475	0.10381
	13	42.699	0.46931	42.633	0.47298	42.614	0.47342	42.596	0.47217
	14	43.109	0.43360	43.063	0.44466	43.06	0.43808	43	0.44673
	15	43.346	0.43301	43.4	0.44864	43.36	0.44153	43.364	0.45392
	16	43.677	0.41442	44.034	0.35287	44.136	0.35861	44.036	0.34081
	17	43.882	0.36443	44.248	0.34382	44.338	0.33443	44.2	0.29612
	18	44.201	0.39087	45.853	0.07761	45.854	0.08132	44.608	0.43507
	19	45.878	0.05857	47.474	0.44554	47.497	0.44250	45.98	0.07872
	20	47.842	0.44711	47.801	0.37125	47.752	0.37096	47.591	0.43719
	21	48.25	0.38055	47.893	0.35427	47.87	0.36176	47.954	0.40277
	22	48.426	0.33643	48.113	0.35268	48.12	0.33653	48.227	0.33298
	23	48.889	0.31375	48.727	0.30233	48.728	0.32163	48.759	0.30838
	24	58.928	0.06715	59.241	0.06237	59.238	0.06256	59.2	0.06212
	25	62.957	0.01403	64.47	0.01639	64.475	0.01802	64.474	0.01648
	26	68.486	0.62437	70.014	0.60995	69.966	0.60818	69.909	0.61002
	27	70.751	0.58770	70.864	0.48709	70.755	0.48158	70.81	0.46047

(Continues)

TABLE 5 | (Continued)

Reference model values				Comp. stage 1 crack		Comp. stage 2 crack		Comp stage 3 crack	
Rot. Vel.	Mode #	Freq (Hz)	Deformation (m)	Freq (Hz)	Deformation (m)	Freq (Hz)	Deformation (m)	Freq (Hz)	Deformation (m)
	28	70.915	0.45739	71.128	0.44442	71.036	0.44314	71.066	0.41495
	29	71.033	0.44401	71.713	0.45550	71.647	0.48162	71.624	0.47143
	30	71.276	0.43663	71.99	0.36868	71.932	0.40347	71.919	0.39622

The observation of peak vibration at natural frequency of turbo-compressor FEA model was made by Moore [9] that is in-line with current work. Similar results of new mode generation and existing mode diminishing were obtained in [8]. Modal Analysis of damped flywheel was done for mode shapes and critical speed identification [20]. The authors carried out modal analysis of flywheel and found natural frequencies by selecting 6 mode shapes. Moreover, the authors obtained 02 critical speeds from Campbell diagram along with the information of stability of mode shapes. In the current work 30 modes were selected (to get more accurate results) for modal analysis and 02 critical speed ranges were found for the representative machine.

3.5 | Harmonic Response Analysis

3.5.1 | Harmonic Response Analysis of Models With Unbalance

Vibration patterns of different models are shown in Figure 5. It was noted that vibration pattern and critical speed ranges remained same in all cases, but vibration amplitude increased proportionally as unbalance mass was increased (Figure 5). For example, vibration amplitudes of model having unbalance 0.005 kg at both critical speeds were 0.0057077 and 0.0109190 m/s. Similarly, vibration amplitudes of model having unbalance 0.05 kg at both critical speeds were 0.0570770 and 0.1091900 m/s. The ratio of unbalance masses of models having unbalance mass of 0.005 and 0.05 kg is 10 and ratio of increase in vibration amplitude at both critical speeds is also 10. The similar vibration response of rotor in case of unbalance was observed [28]. Maximum vibration amplitude was observed at 48 Hz. It is construed from here that if vibration amplitudes are increased but the critical speed ranges are not changed in actual machine, it will point to unbalance (Table 6).

Vibration response of rotor with unbalance has been worked out by Yang and the results were similar [16]. Similar results for motorized spindle system were obtained by Xul [14]. Below comparison is drawn for the current work with already published work.

This led to the apprehension of the fact that with an increase in vibration amplitudes at same critical speeds, the scenario would be pointing to unbalance in real machine.

Similarly, maximum deformation was observed in the second critical speed range as shown in Figure 6. Deformation response was also found linear to unbalance mass.

Modal analysis and harmonic response analysis of high-pressure rotor support system was done for damping optimization, and the results were same; that is, vibration and deformation were maximum near critical speed [21]. The same results were obtained in the current work. The reason behind the similar results is that in critical speed zones, resonance is occurring. It means that impact created due to matching of natural frequencies of the systems in operation is very huge. This impact causes maximum vibration as well as maximum deformation in the critical speed regions.

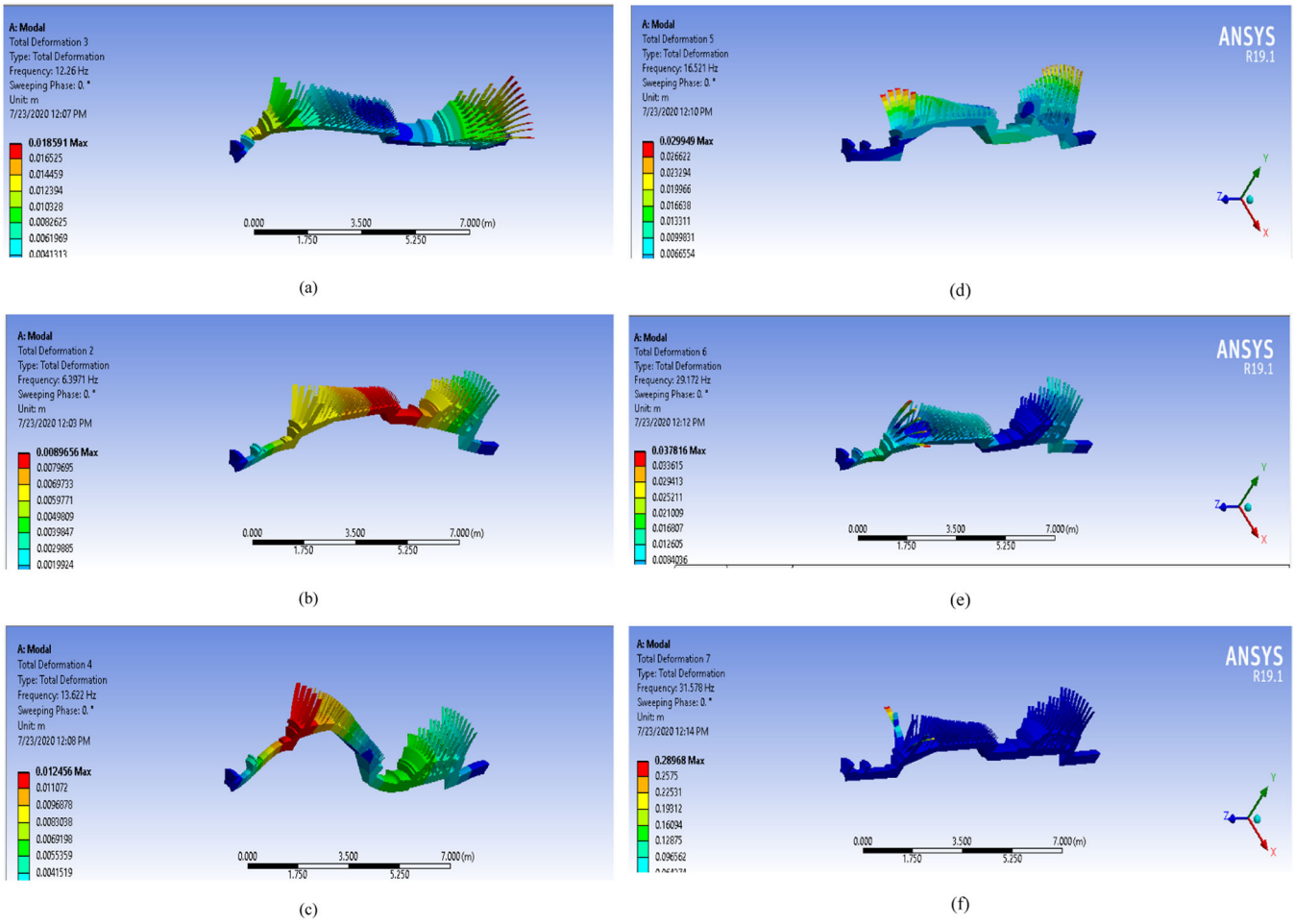

FIGURE 4 | Sample mode shapes indicating total deformation and frequency.

3.5.2 | Harmonic Response Analysis of Models With Crack and Without Unbalance

Vibration patterns of models with crack are shown in Figure 7. Maximum vibration amplitude observed during the first critical speed range while vibrations amplitudes in second critical speed range are lesser than that of first critical speed range vibration amplitudes. However, it was noted that critical speed ranges remained the same. This shift of maximum vibration amplitude frequency was key finding in case of crack in reference model. Same shift in deformation pattern was observed as indicated by Figure 8.

It was noted that there was no correlation of vibration amplitude among all these cases. This is due to dynamic response of models. Even models having crack on the same stage, but different blade were presenting different response to crack in dynamic conditions. Shifting of high vibration frequency in case of crack in rotor was also observed but this was in sub critical zone [28]. By comparing model without unbalance and crack with model having crack but without unbalance, it was noted that vibration level was significantly increased. There was no correlation between vibration level of model without crack and model having crack.

3.5.3 | Vibrations Pattern With Unbalance and Crack

Results of different scenarios are discussed in the sections below.

3.5.3.1 | Harmonic Response Analysis: When Crack Location Was Changed in Different Stages. It was observed that if crack location was changed from one stage to other, vibration pattern remained same as shown above in case of cracks only models (Figure 7). So, maximum amplitude frequency remained same but change in vibration amplitude was observed as shown in Figure 9.

Crack behavior dominated over unbalance behavior as maximum vibration amplitude occurred during the first critical speed range. It was observed that combined impact of unbalance and crack was more than the sum of unbalance and crack impact when impacting individually. For example, first critical speed vibration amplitude of model with unbalance and without crack was 0.0057077 m/s while first critical speed vibration amplitude of model without unbalance and with crack was 0.0000000168 m/s. The simple sum of these values is 0.005707717 m/s while vibration amplitude of model having crack and unbalance was 0.016756 m/s. This value is 0.011048283244 m/s more than simple

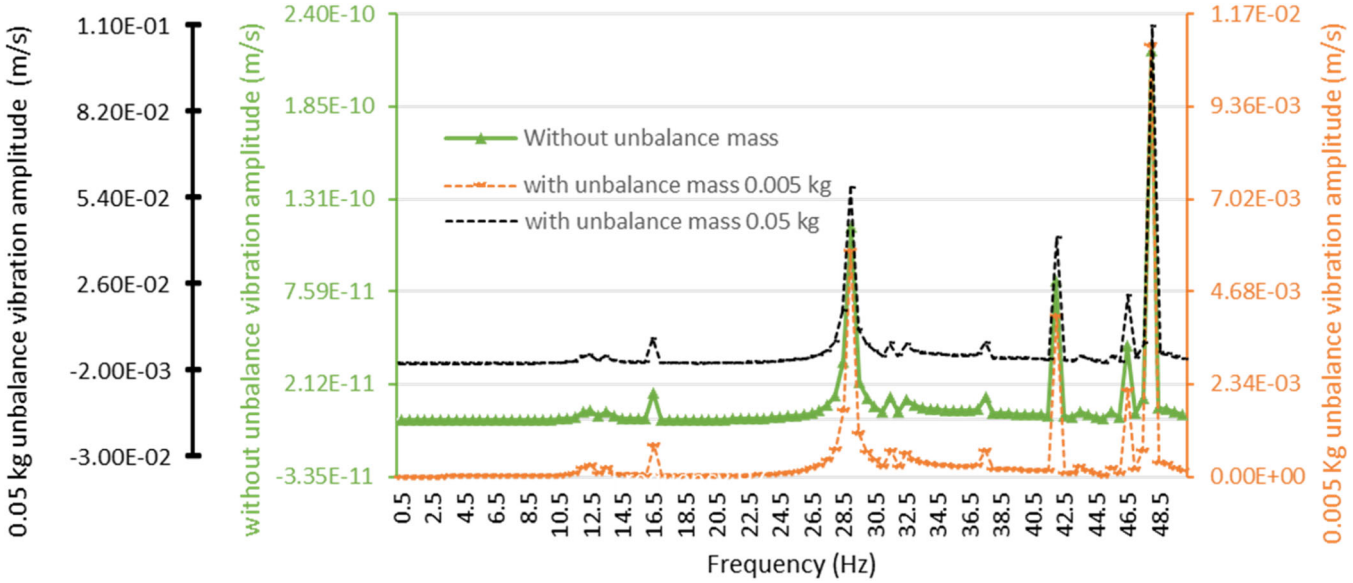

FIGURE 5 | Harmonic response analysis results of models with unbalance and without crack.

TABLE 6 | Comparison of work with already published work.

Current work outcome	Already published work results	Remarks
Vibration amplitude increases with unbalance	Synchronous Vibration amplitude increases with unbalance [4]	Both findings are similar
Vibration amplitude behavior is linear with unbalance	Vibration amplitude behavior is linear with unbalance [13]	Both findings are similar
Critical speeds remained same	Critical speeds for different unbalances remained almost same [15]	Both findings are different
No change in critical speed	In case of out of phase unbalance case, critical speed increases with unbalance [15]	This finding is different than current work due to nature of unbalance.

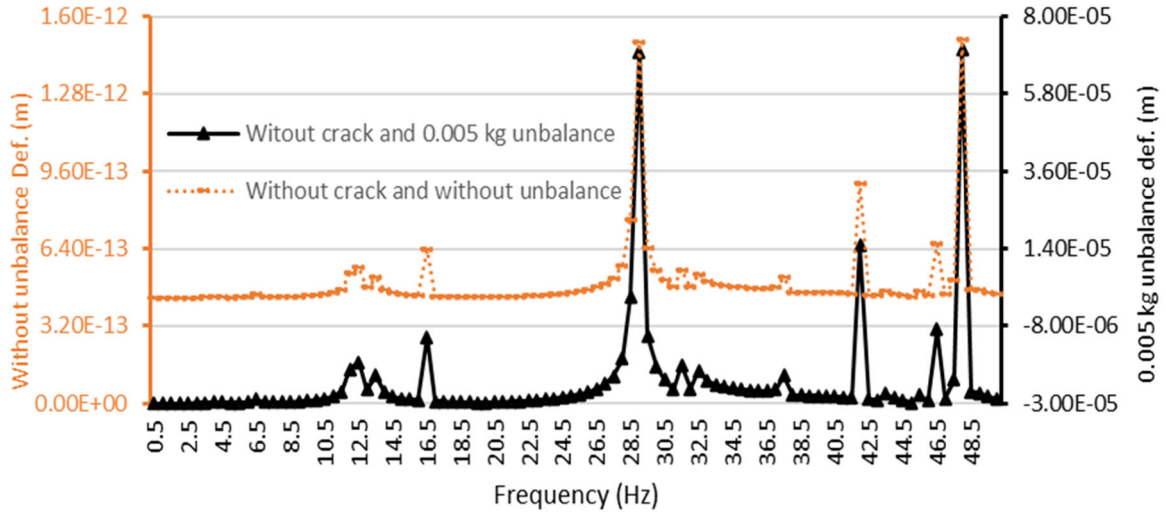

FIGURE 6 | Deformation response of models without crack.

sum value. This was due to the dynamic response of the machine. Simply, we can say that crack with unbalance behavior was amplification of crack behavior. If the system has built in unbalance as its possible in most of actual machines, this behavior would help to point out the problem at very initial stage.

3.5.4 | Harmonic Response Analysis: When Crack Location Was Changed in Same Stage

Vibration patterns of models with inherent unbalance and different crack locations are shown in Figure 10. It was seen that vibration

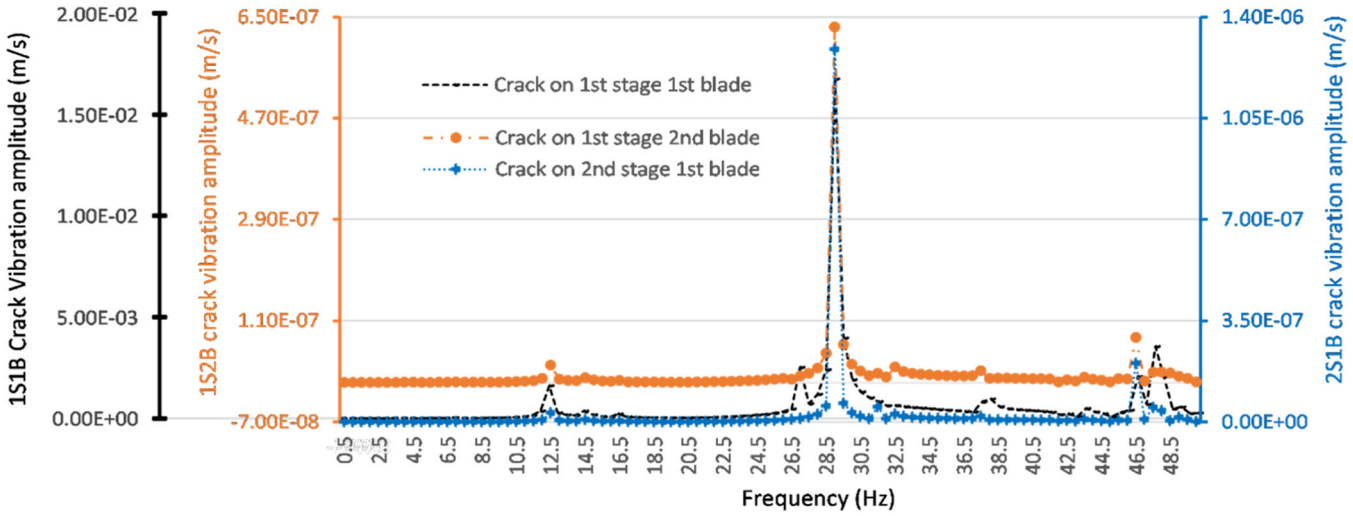

FIGURE 7 | Harmonic response analysis results of models without unbalance and having crack.

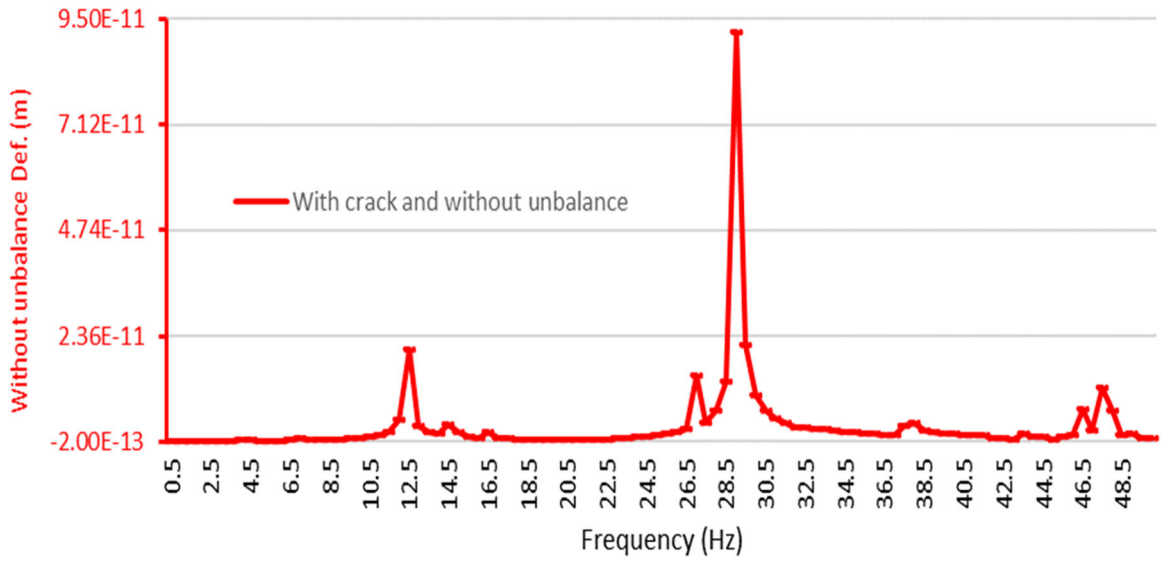

FIGURE 8 | Deformation response of model with crack and without unbalance.

amplitude of model having crack location nearer to unbalance location was higher than models having crack and unbalance at distant locations (Figure 10). Maximum vibration amplitude frequency remained same while pattern was changed.

As the crack location got closer to unbalance mass, vibration amplitude increased. When crack location is distant from unbalance location, vibration amplitude reduction was observed. All this was due to dynamic response of the system. When crack and unbalance locations are closer dynamic response severity was higher than that of distant locations of unbalance and crack model.

3.5.5 | Harmonic Response Analysis: When Unbalance Mass Was Changed Without Changing Crack Location

In this case, change in vibration amplitude was found directly proportional to change in unbalance mass while pattern remained same. Results of various models are provided in Table 7. This behavior can be applied to the case where crack has initiated, its either detected or not but rectification is not done. In such instances, if further unbalance is created due to any reasons like material liberation, this type of behavior, as discussed above, would be observed indicating that situation is worsening further in real machine.

3.5.6 | Harmonic Response: Models With Different Crack Thickness and Crack Depth

It was seen that maximum vibration frequency shifted from 48 to 29 Hz in model with inherent unbalance and crack of 1 mm thickness. As the crack further propagated and its depth increased from 31 to 372 mm with an increment of 31 mm, maximum vibration amplitude frequency remained 29 Hz. But upon further increase in crack depth to 403 mm, while its thickness was still 1 mm, maximum vibration frequency was

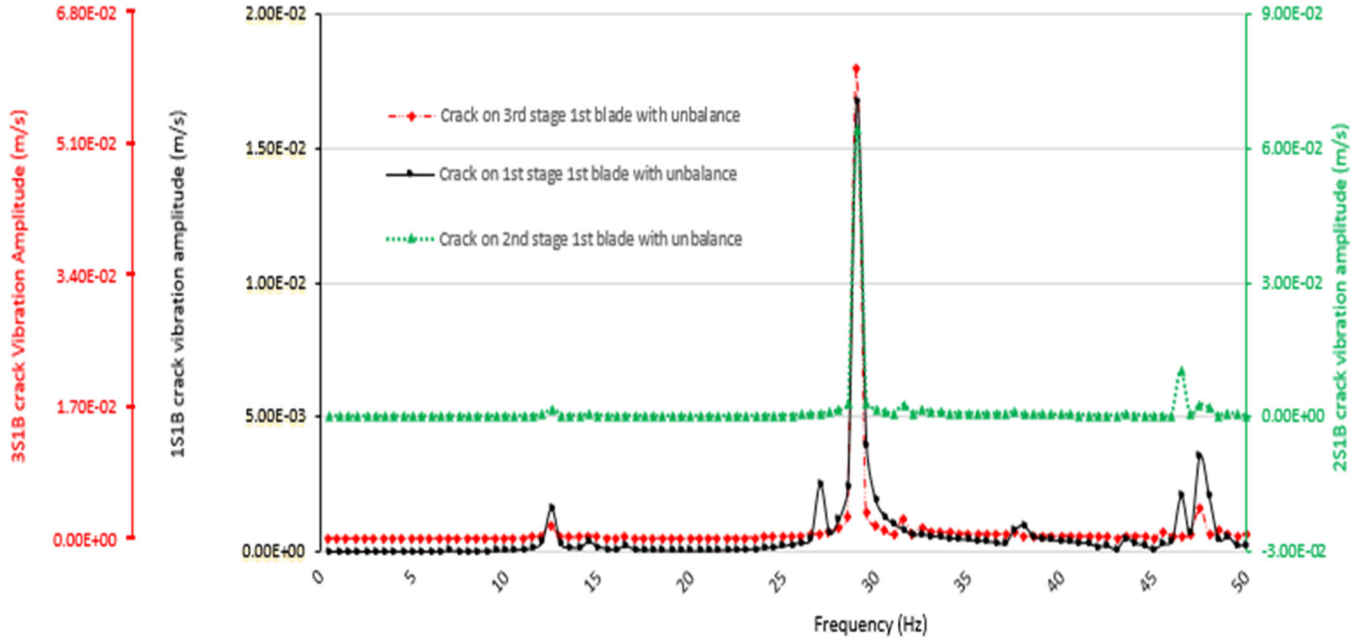

FIGURE 9 | Harmonic response analysis results of different models with crack and unbalance at different locations.

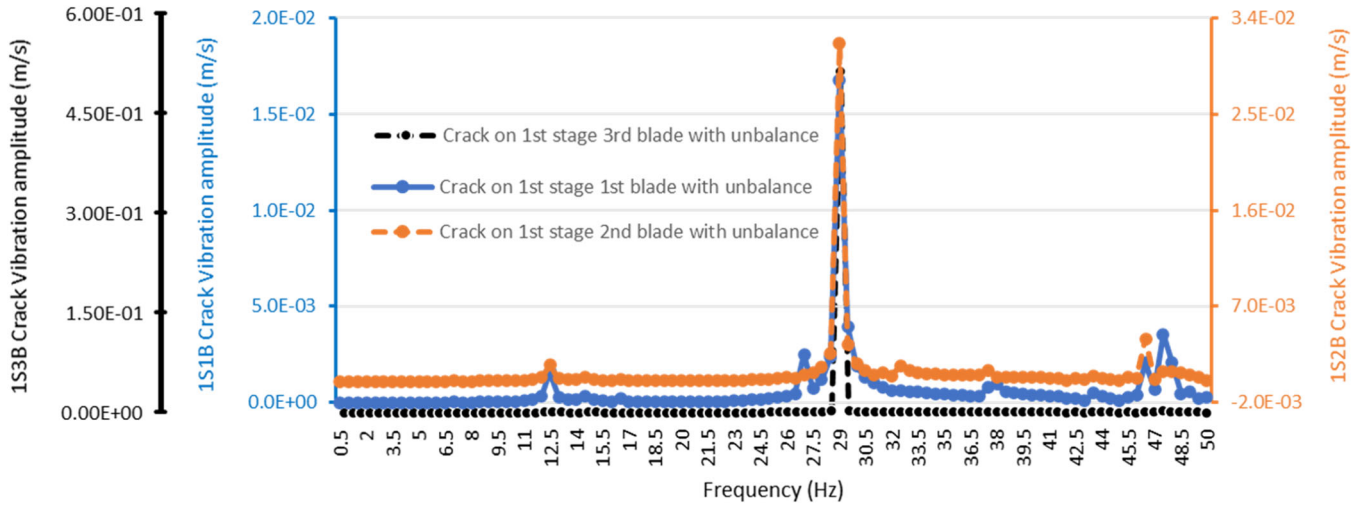

FIGURE 10 | Harmonic response analysis results of different models with crack and having unbalance at different locations but at the same stage.

TABLE 7 | Summary of unbalance mass with crack behavior.

Unbalance mass (kg)	Vibration amplitude (m/s)	Ratio of unbalance mass	Ratio of vibration amplitudes
0.01	3.3512E−02		
0.025	8.3779E−02	2.5	2.5
0.05	0.16756	2.0	2.0

reverted to 48 Hz. This reversal in frequency may be due to the release of energy due to the crack.

If crack thickness was increased from 1 to 3 mm with an increment of 1 mm, the maximum vibration frequency remained 29 Hz. The vibration amplitude of the model with a crack at the middle of blade was higher than the vibration of models with crack at the top and bottom of blade in the case of 1 mm crack thickness. This result was similar to the work reported in [28]. As per El-Mongy's work, vibration amplitude of the system having crack with misalignment is lesser than that of crack only, but in the current work, vibration amplitude of the system having crack with unbalance is more than that of crack only. The reasons for the difference may be unbalance amplifies the fault while misalignment sometimes compensates the vibration amplitude.

For 2 and 3 mm crack thickness, the maximum vibration amplitude was observed in the model with the crack at the bottom of the blade. Vibration results for 2 and 3 mm thick crack with change in location were as expected as crack at the root has much impact than other location due to high stress concentration. Vibration results for 1 mm thick crack with change in location were unexpected. This may be because in case of small cracks, as the stiffness of structure is more than the impact caused by the crack, energy is dissipated and vibration amplitudes are not increased but for such kind of cracks, vibration amplitudes are higher at far location from the root/fixed location.

3.6 | Identification of Critical Speeds Beyond Operating Limit

Campbell diagram of the model for identification of third and fourth critical speed ranges is shown in Figure 11. As per Campbell diagram, it can be seen that first and second critical speed ranges remain same as mentioned in Table 4 that proved the accuracy of the developed numerical model.

The third and fourth critical speed ranges were identified as from 3601 to 3864 rpm and 4113 to 4279 rpm, respectively. Third critical speed range was observed nonlinear. As these critical speed ranges were well beyond the operating speed. Therefore, currently, there was no chance of resonance due to these natural frequencies. It is believed from the data that if crack is initiated and it causes reduction of natural frequency, even then operating range would be much lower than reduced natural frequency. As first and second critical speed ranges were already lower than operating speed, hence chances of resonance due to reduction in natural frequency caused by crack would be very remote.

3.7 | Flow Induced Vibration Based Pulsations

Graphs of casing vibration and rotor vibration are shown in Figure 12. This graph is particularly important to trend the behavior of machines. This graph considers both rotor and casing vibration. Any change in either casing or rotor vibration may be due to excitation of flow induced vibrations (FIVs) based pulsations. These pulsations would be of very short duration and high intensity. These FIVs-based pulsations usually occur in transient conditions, that is, load ramp up or ramp down from stable load.

It is evident that vibration remained stable indicating there were no FIV-based pulsations in the blades at different loads. The obtained results are different than the results reported in [33]. The future trending of this behavior would also be useful to highlight FIVs-based pulsations in blades if occurring. Therefore, this graph would also help pinpoint the one cause of vibration; FIVs-based blade pulsations. The similar results were expected as there should be no FIV-based pulsations in the new machine. Such kinds of pulsations are never expected at such an initial stage.

3.8 | Nonlinearity Analysis

The Hilbert Transform (HT) graph, as illustrated in Figure 13, provides a comprehensive analysis of the system's dynamic response across different frequency ranges. The results indicate that the system exhibits predominantly linear behavior up to its designated operating frequency, confirming stable and predictable performance within this range. However, beyond this threshold, a slight non-linear system response is observed but this deviation is not a concern, as the machine is neither expected to reach nor operate at such high speeds under normal

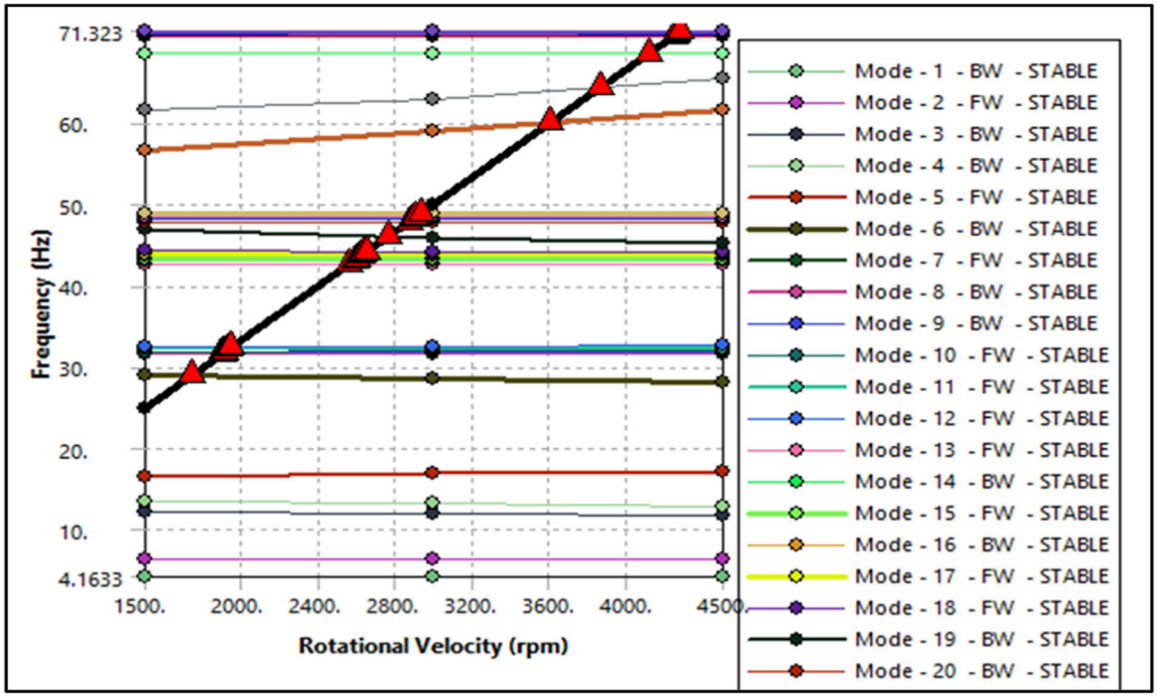

FIGURE 11 | Campbell diagram for third critical speed identification.

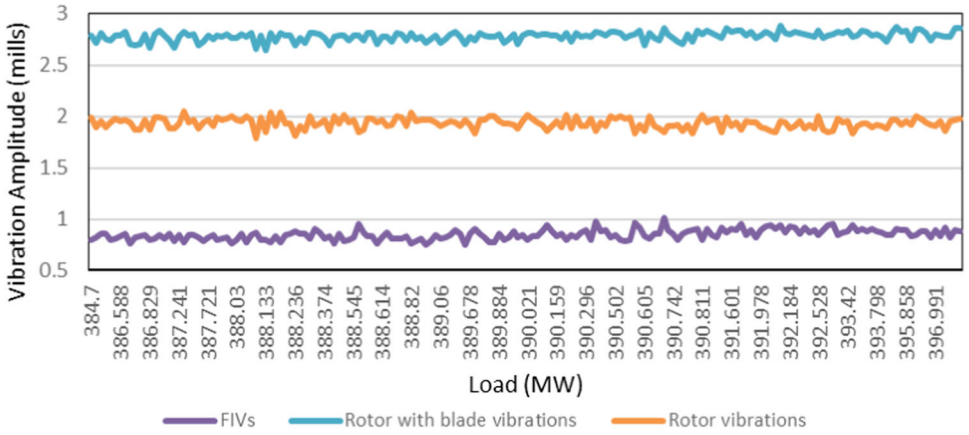

FIGURE 12 | Flow induced vibrations based pulsation effects graph.

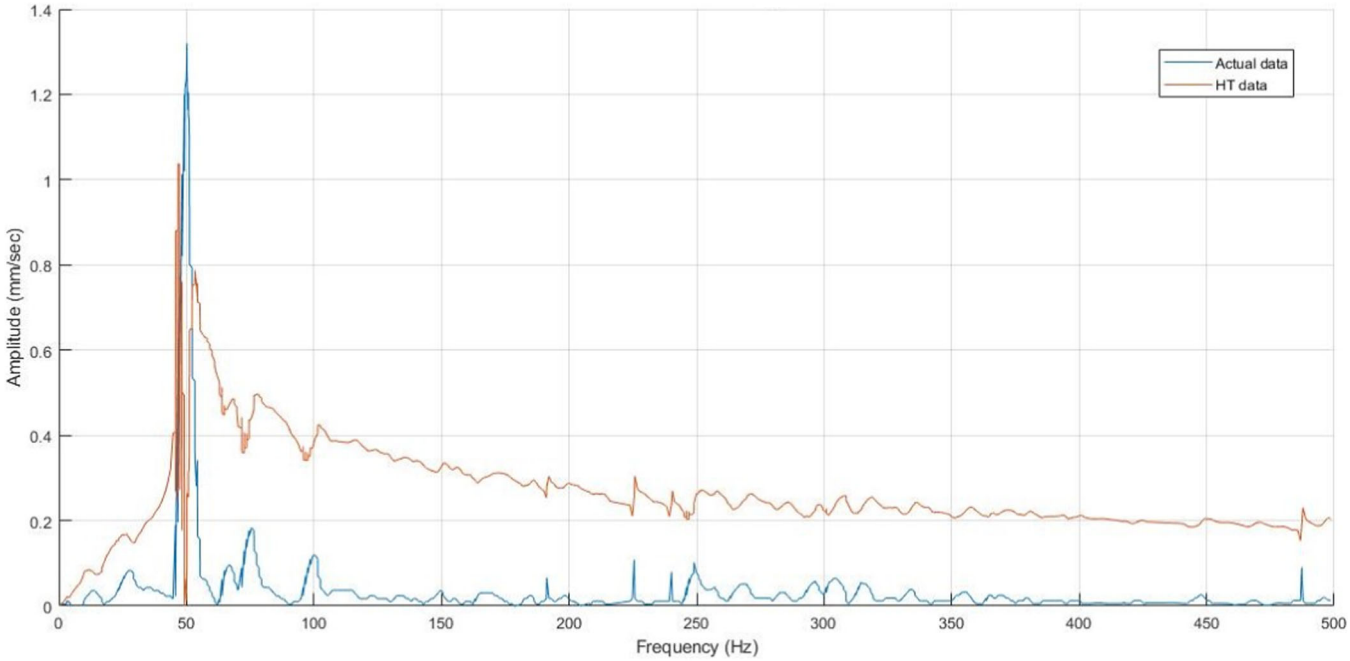

FIGURE 13 | Nonlinearity analysis through Hilbert transform for Nonlinearity Analysis.

conditions. Furthermore, the rotodynamic behavior of the machine remains consistent over time, with no observable changes throughout the monitoring period. This stability implies that no mechanical abnormalities, wear, or deterioration have occurred, thereby reinforcing the reliability of dynamic system. Given this stability, the present Hilbert Transform analysis serves as a robust baseline for future diagnostics. Establishing such a reference enables early identification of deviations in the system's dynamic response, facilitating predictive maintenance and ensuring long-term operational integrity.

The findings of this study align with the work of Feldman et al. [29], who also employed HT for identifying nonlinearity in dynamic systems. The consistency between the current analysis and Feldman's work further substantiates the validity of HT as an effective analytical tool for tracking system behavior. These results further support the application of HT in condition monitoring, where continuous assessment of nonlinear characteristics can aid in early fault detection and system optimization.

3.9 | Material Properties Uncertainty Analysis

Percentage change in natural frequency of models with different Young's modulus is shown in Figure 14. It can be seen that percentage change in frequency at different modes is half than percentage variation of Young's Modulus of different models from reference models.

Similarly, change in frequency with variation in material Young's modulus at different elements of different models is described in Figure 15. Variation in frequency at different modes was 1/4th (25%) of the change in Young's modulus of different models.

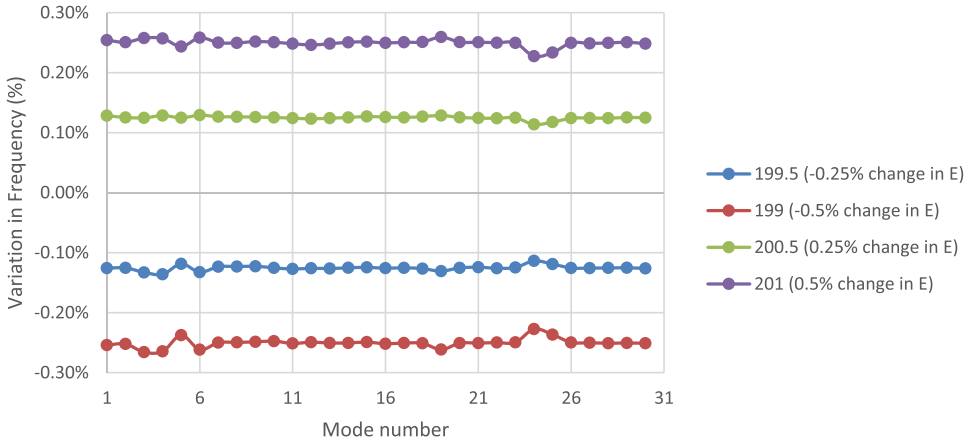

FIGURE 14 | Effect of material Young's modulus variation on natural frequency variations.

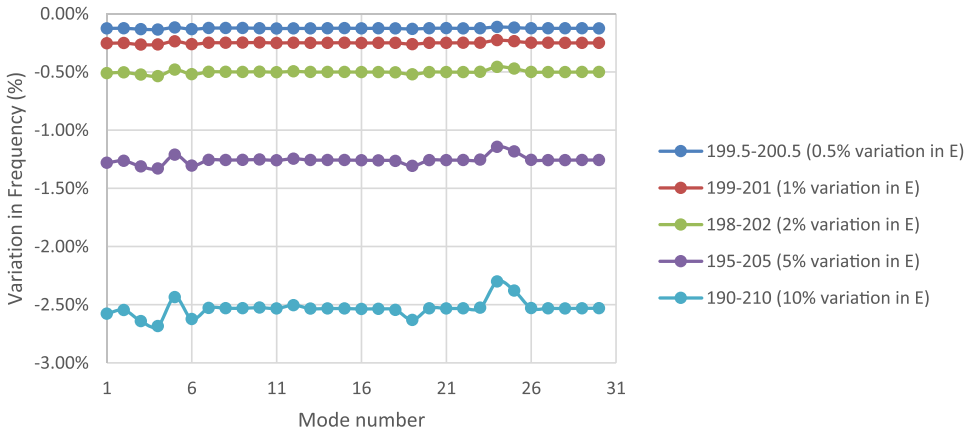

FIGURE 15 | Variation in natural frequency with variation in material Young's modulus at different modes.

4 | Conclusions

Modal and Harmonic response analyses of gas turbine rotor under various scenarios were carried out and compared with actual response of machine to predict the crack initiation, unbalance and both right at the inception stage. Three scenarios; unbalance, crack with balance and combined unbalance and crack models were developed and analyzed for fault detection. Key findings of work were.

1. In case of unbalance in rotor, direct relation between change in unbalance mass and change in vibration amplitude was observed while critical speed ranges and vibration pattern remained same. Maximum vibration amplitude frequency remained the same. This relation was found valid for unbalance mass range 1.0×10^{-9} to 0.05 kg.
2. For crack (1–3 mm thickness and depth up to 372 mm) at any blade, shift in maximum vibration amplitude frequency to first critical speed, that is, 29 Hz from second critical speed, that is, 48 Hz was noted while critical speed ranges remained same. As increase in vibration amplitude was under alarm limit, it could not be detected by conventional vibration monitoring systems. However, the devised method would detect this anomaly.
3. Models with crack at the bottom of the blade were found more sensitive than models with crack at the middle or at the top of blade for crack thickness of 2 and 3 mm. However, vibration caused by 1 mm thickness crack at the bottom of blade was suppressed at the fixed end of blade.
4. In the presence of inherent unbalance and crack on blade, cracks behavior dominance was observed.
5. In the presence of inherent unbalance and crack on blades when the location of unbalance and crack were at different stages, the maximum vibration frequency and vibration pattern remained same as of reference model irrespective of the crack location.
6. In the presence of inherent unbalance and crack on blades when the location of unbalance and crack were at the same stage, the maximum vibration frequency remained the same as of the reference model while the change in vibration pattern was observed.
7. In the case of further unbalance in addition to inherent unbalance with crack, change in vibration amplitude was directly proportional to the change in unbalance mass.
8. New modes with different mode shapes and natural frequencies were observed in case of crack. Similarly, shifting of modes was also observed in different cases of crack.

The devised method to develop, compare with actual machine and then use of results for different simulated abnormal conditions would be very useful to identify the potential faults at their inception stage before they may cause damage to machines or unplanned shutdown. Basic procedure would remain the same but machine-specific changes of unbalance mass to be done for other machines based on their actual behavior rather than doing analysis on design parameters that would not depict the actual machine behavior.

This work can be further extended to investigate machine behavior in case of multiple unbalances, multiple cracks, blade looseness and misalignment.

Conflicts of Interest

The authors declare no conflicts of interest.

References

1. N. Teyi and S. Singh, "A Decadal Review of Various Modelling and Analysis of Cracked Rotors," *Procedia Structural Integrity* 39 (2022): 333–346.

2. A. Abbasi, F. Nazari, and C. Nataraj, "Adaptive Modeling of Vibrations and Structural Fatigue for Analyzing Crack Propagation in a Rotating System," *Journal of Sound and Vibration* 541 (2022): 117276.

3. R. X. Perez, *Design, Modeling and Reliability in Rotating Machinery* (John Wiley & Sons, 2022).

4. N. Aimeur and N. Menasri, "Computational Investigation of Vibration Characteristics Analysis for Industrial Rotor," *Acta Mechanica et Automatica* 16, no. 4 (2022): 373–381.

5. P. A. Chandran and C. P. S. Kumar, "Vibration Analysis of Rotating Pre-Twisted Curved Blades Under Thermal Environment," *International Journal of Dynamics and Control* 11, no. 3 (2023): 919–927.

6. A. Bovsunovsky and O. Nosal, "Highly Sensitive Methods for Vibration Diagnostics of Fatigue Damage in Structural Elements of Aircraft Gas Turbine Engines," *Procedia Structural Integrity* 35 (2022): 74–81.

7. G. E. Gongwei, D. Huiliang, and P. Yitian, "Critical Speed Analysis of Rotor System of Sealing Machine," *Journal of Physics: Conference Series* 1939, no. 1 (2021): 012090.

8. S. Chan, H. Liu, F. Xing, and H. Song, "Wave Rotor Design Method With Three Steps Including Experimental Validation," *Journal of Engineering for Gas Turbines and Power* 140, no. 11 (2018): 111201.

9. J. T. Gravdahl and O. Egeland, "A Moore-Greitzer Axial Compressor Model With Spool Dynamics," in *Proceedings of the 36th IEEE Conference on Decision and Control*, Vol. 5 (IEEE, 1997), 4714–4719.

10. S. Doshi, A. Katoch, A. Suresh, et al., "A Review on Vibrations in Various Turbomachines Such as Fans, Compressors, Turbines and Pumps," *Journal of Vibration Engineering & Technologies* 9, no. 7 (2021): 1557–1575.

11. A. Shrivastava and A. R. Mohanty, "Identification of Unbalance in a Rotor-Bearing System Using Kalman Filter–Based Input Estimation Technique," *Journal of Vibration and Control* 26, no. 11–12 (2020): 1081–1091.

12. A. T. Watban Khalid Fahmi, K. Reza Kashyzadeh, and S. Ghorbani, "A Comprehensive Review on Mechanical Failures Cause Vibration in the Gas Turbine of Combined Cycle Power Plants," *Engineering Failure Analysis* 134 (2022): 106094.

13. Z. Hu, Y. Yang, C. Zhou, X. Zheng, and R. Li, "On the Symplectic Superposition Method for New Analytic Free Vibration Solutions of Side-Cracked Rectangular Thin Plates," *Journal of Sound and Vibration* 489 (2020): 115695.

14. Y. Song, K. Xue, and Q. Li, "A Solution Method for Free Vibration of Intact and Cracked Polygonal Thin Plates Using the Ritz Method and Jacobi Polynomials," *Journal of Sound and Vibration* 519 (2022): 116578.

15. Z. Hu, Y. Shi, S. Xiong, X. Zheng, and R. Li, "New Analytic Free Vibration Solutions of Non-Lévy-Type Porous FGM Rectangular Plates Within the Symplectic Framework," *Thin-Walled Structures* 185 (2023): 110609.

16. Y. Yang, J. Wang, X. Wang, and Y. Dai, "A General Method to Predict Unbalance Responses of Geared Rotor Systems," *Journal of Sound and Vibration* 381 (2016): 246–263.

17. L. B. Saint Martin, L. L. Gusmão, T. H. Machado, E. P. Okabe, and K. L. Cavalca, "Operational Modal Analysis Application to Support Structure Identification Under Rotating Machinery Unbalance," *Engineering Structures* 249 (2021): 113344.

18. C. Veera Sesha Kumar, E. K. Vivek, and S. Vignesh, "Rotordynamic Analysis and Redesign of High-Pressure Turbine Test Rig," in *Proceedings of the 6th National Symposium on Rotor Dynamics: NSRD 2019* (Springer, 2021), 77–91.

19. N. S. Pirogova and P. A. Taranenko, "Calculative and Experimental Analysis of Natural and Critical Frequencies and Mode Shapes of High-Speed Rotor for Micro Gas Turbine Plant," *Procedia Engineering* 129 (2015): 997–1004.

20. M. T. Hamisu, U. S. Umar, and A. Sa'ad, "FEA and Modal Analysis of a Damped Flywheel With Unbalanced Masses," *Applications of Modelling and Simulation* 4 (2020): 21–30.

21. L. Shuming and W. Yujia, "Damping Optimization of High Pressure Rotor Support Based on Harmonic Response Analysis," *Journal of Physics: Conference Series* 1861, no. 1 (2021): 012112.

22. H. I. Mansoora, M. Al-Shammari, and A. Al-Hamood, "Theoretical Analysis of the Vibrations in Gas Turbine Rotor," *IOP Conference Series: Materials Science and Engineering* 671, no. 1 (2020): 012157.

23. M. S. Taima, T. A. El-Sayed, M. B. Shehab, S. H. Farghaly, and R. J. Hand, "Vibration Analysis of Cracked Beam Based on Reddy Beam Theory by Finite Element Method," *Journal of Vibration and Control* 29, no. 19–20 (2023): 4589–4606.

24. M. Mohtasham Khani, S. Vahidnia, L. Ghasemzadeh, et al., "Deep-Learning-Based Crack Detection With Applications for the Structural Health Monitoring of Gas Turbines," *Structural Health Monitoring* 19, no. 5 (2020): 1440–1452.

25. Y. Chen, D. An, C. Zhou, Y. Li, J. Xu, and R. Li, "Analytical Free Vibration Solutions of Rectangular Edge-Cracked Plates by the Finite Integral Transform Method," *International Journal of Mechanical Sciences* 243 (2023): 108032.

26. E. L. Sh, S. Kattimani, and N. Thoi Trung, "Frequency Response Analysis of Edge-Cracked Magneto-Electro-Elastic Functionally Graded Plates Using Extended Finite Element Method," *Theoretical and Applied Fracture Mechanics* 120 (2022): 103417.

27. U. Ehehalt, O. Alber, R. Markert, and G. Wegener, "Experimental Observations on Rotor-to-Stator Contact," *Journal of Sound and Vibration* 446 (2019): 453–467.

28. H. H. El-Mongy and Y. K. Younes, "Vibration Analysis of a Multi-Fault Transient Rotor Passing Through Sub-Critical Resonances," *Journal of Vibration and Control* 24, no. 14 (2018): 2986–3009.

29. M. Feldman, "Hilbert Transform Methods for Nonparametric Identification of Nonlinear Time Varying Vibration Systems," *Mechanical Systems and Signal Processing* 47, no. 1–2 (2014): 66–77.

30. A. Hu, L. Xiang, and Y. Zhang, "Experimental Study on the Intrawave Frequency Modulation Characteristic of Rotor Rub and Crack Fault," *Mechanical Systems and Signal Processing* 118 (2019): 209–225.

31. Y. Jia, Y. Liu, Q. Wang, M. Li, and J. Li, "Nonlinear Dynamics Analysis on Intermediate Bearing-Dual Rotor System for a Marine Gas

Turbine," *IOP Conference Series: Earth and Environmental Science* 510, no. 2 (2020): 022031.

32. N. Wang, C. Liu, D. Jiang, and K. Behdinan, "Casing Vibration Response Prediction of Dual-Rotor-Blade-Casing System With Blade-Casing Rubbing," *Mechanical Systems and Signal Processing* 118 (2019): 61–77.

33. M. Agrawal and R. Krishnadutt, "Fluid Induced Vibrations in Rotors Supported by Journal Bearings: A Case Study," in *Asset Intelligence Through Integration and Interoperability and Contemporary Vibration Engineering Technologies: Proceedings of the 12th World Congress on Engineering Asset Management and the 13th International Conference on Vibration Engineering and Technology of Machinery* (Springer, 2019), 31–40.